# Interaction of a Cumulus Cloud Ensemble with the Large-Scale Environment. Part IV: The Discrete Model

STEPHEN J. LORD,[1] WINSTON C. CHAO[2] AND AKIO ARAKAWA

*Department of Atmospheric Sciences, University of California, Los Angeles 90024*

(Manuscript received 26 August 1980, in final form 21 September 1981)

ABSTRACT

An application of the Arakawa-Schubert (1974) cumulus parameterization to a prognostic model of the large-scale atmospheric circulations is presented. The cloud subensemble thermodynamical properties are determined from the conservation of mass, moist static energy and total water (vapor, suspended liquid water and precipitation). Algorithms for calculating the large-scale forcing and the mass flux kernel are presented. Several methods for solving the discrete version of the integral equation for the cumulus mass flux are discussed. Equations describing the cumulus feedback on the large-scale thermodynamical fields are presented.

## 1. Introduction

A cumulus cloud parameterization for use in large-scale numerical prediction models has been presented in Part I of this series of papers (Arakawa and Schubert, 1974). The closure assumption for the parameterization, the cloud-work function quasi-equilibrium, has been examined using observations in Part II (Lord and Arakawa, 1980) and the entire parameterization has been evaluated using a semi-prognostic approach applied to GATE Phase III data in a companion paper in this issue (Lord, 1982, hereafter referred to as Part III). The present paper describes an application of the Arakawa-Schubert parameterization to a prognostic model of the large-scale atmospheric circulations. This discretized form of the parameterization has been incorporated into the UCLA general circulation model (GCM) and has been used to analyze observed data in Parts II and III.

Section 2 summarizes the vertical structure of the discrete model and the solution procedure for the cloud subensemble thermodynamical properties. Section 3 introduces the discrete form of the integral equation for the mass flux distribution function and outlines procedures for calculating the large-scale forcing and the mass flux kernel. Section 4 describes several methods for solving the discrete form of the mass flux distribution equation. Section 5 presents the discrete equations describing the cumulus feedback on the large-scale fields in the discrete model. The Appendix includes details omitted from the main body of the paper.

## 2. The vertical structure of the discrete model and the solution for the cloud subensemble thermodynamical properties

Fig. 1 shows the vertical structure of the large-scale model. Pressure $p$ is used as the vertical coordinate. The dashed lines indicate levels with integer index $k$ where the large-scale temperature $\bar{T}(k)$ and water vapor mixing ratio $\bar{q}_v(k)$ are predicted. The solid lines indicate half-integer levels where the large-scale vertical $p$ velocity $\bar{\omega}$ is defined. The region bounded by levels $k - \frac{1}{2}$ and $k + \frac{1}{2}$ is referred to as "layer $k$".

In numerical prediction models some preadjustments of the large-scale thermodynamical structure must be made before the cumulus parameterization is applied. The parameterization assumes that all layers of the large-scale environment are at least neutral with respect to dry convection. This assumption requires that the large-scale dry static energy $\bar{s} = c_p\bar{T} + gz$ does not decrease with height, i.e.,

$$\bar{s}(k) \leq \bar{s}(k-1) \quad \text{for} \quad 2 \leq k \leq KM, \qquad (1)$$

where $KM$ is the index of the lowest model layer. When this requirement is not satisfied a dry convective adjustment is performed.

The following vertically interpolated variables are supplied by the large-scale model at all half-integer levels: $\bar{T}(k+\frac{1}{2})$, $\bar{q}_v(k+\frac{1}{2})$, $z(k+\frac{1}{2})$ (the height above sea level) and $\bar{q}_v^*(k+\frac{1}{2})$ (the saturation water vapor mixing ratio). Interpolations of these variables

[1] Current affiliation: Atlantic Oceanographic and Meteorological Laboratories, National Hurricane Research Laboratory, NOAA, Coral Gables, FL 33146.

[2] Current affiliation: Science Applications Inc., McLean, VA 22102.

0022-4928/82/010104-10$06.50

© 1982 American Meteorological Society

Unauthenticated | Downloaded 12/05/22 01:05 AM UTC

to half-integer levels must not create any computational subgrid-scale dry convective instability or any computational subgrid-scale moist convective instability (Conditional Instability of the Computational Kind, Arakawa and Lamb, 1977).

In this application of the parameterization the integer level mixing ratio $\bar{q}_v(k)$ and moist static energy $\bar{h}(k)$ are treated as layer-averaged quantities

$$\bar{q}_v(k) = \tfrac{1}{2}[\bar{q}_v(k - \tfrac{1}{2}) + \bar{q}_v(k + \tfrac{1}{2})]$$

and

$$\bar{h}(k) = \tfrac{1}{2}[\bar{h}(k - \tfrac{1}{2}) + \bar{h}(k + \tfrac{1}{2})]$$

for $2 \leq k \leq KM - 1$. Values for $k = 1$ and $k = KM$ are taken directly from the large-scale variables at the integer levels. The layer-averaged saturation moist static energy $\bar{h}^*(k)$ is calculated from the $\bar{h}(k)$ and $\bar{q}_v(k)$ given above and from $z(k)$ given by the large-scale model. Virtual temperature effects are not discussed here for simplicity but they can be included in a straightforward manner as in Lord (1978).

The lowest model layer $k = KM$ is the subcloud layer (SCL) and the layer $k = KF$ is the layer just above cloud base. The pressure at cloud base, $k = KF + \tfrac{1}{2}$, is denoted by $p_B$ and may be predicted, as in the UCLA GCM, or prescribed, as in the semi-prognostic study presented in Part III. The updrafts at the cloud base have moist static energy

$$h_m \equiv \bar{h}(KM), \tag{2}$$

and water vapor mixing ratio

$$q_{vm} \equiv \bar{q}_v(KM). \tag{3}$$

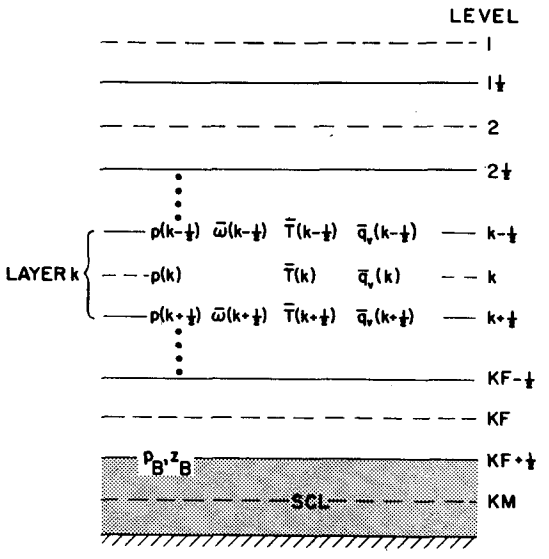


FIG. 1. The vertical structure of the large-scale model. $KM$ is the index of the subcloud layer (shaded) and $KF$ denotes the layer immediately above. Pressure $p$, temperature $\bar{T}$ and mixing ratio $\bar{q}_v$ are provided at both integer and half-integer levels, and vertical velocity $\bar{\omega}$ is given at half-integer levels only.

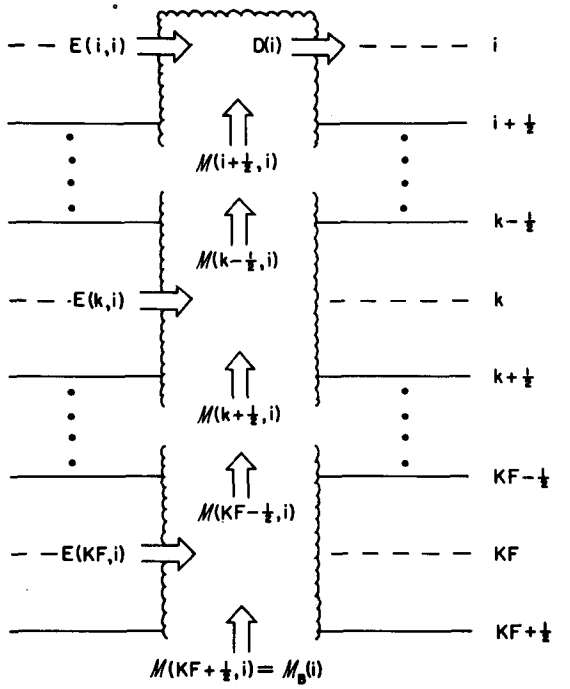


FIG. 2. The vertical structure of the $i$th cloud type. Entrainment $E$ takes place at all integer levels penetrated by the cloud-top including the cloud-top level, while detrainment $D$ takes place at the cloud-top level only. The subensemble vertical mass flux $\eta$ is stored at the half-integer levels and is normalized at cloud base (level $KF + \tfrac{1}{2}$).

For simplicity the presence of stratus clouds in the SCL is neglected here.

When a discrete version of the Arakawa-Schubert parameterization is used in a prognostic model, it is convenient to decompose the cloud ensemble into subensembles according to the cloud-top level (rather than the fractional entrainment rate) as discussed in Part II. Therefore, the cloud top is defined at the integer levels and a cloud which has its top at level $i$, where $1 \leq i \leq KF$, is defined as the $i$th cloud type (Fig. 2). The $i$th cloud type is assumed to be representative of all members of the cloud subensemble with tops in layer $i$. The fractional entrainment rate of the $i$th cloud type is denoted by $\lambda(i)$ and the cloud-top pressure is denoted by $\hat{p}(i)$. Note that $\lambda(i)$ is a dependent variable here, whereas it is taken as an independent variable in the continuous version described in Part I.

The vertical structure of the $i$th cloud type is shown in Fig. 2. Height-dependent cloud-subensemble variables are represented by double arguments throughout this paper. For example, the subensemble vertical mass flux for cloud type $i$, defined at the half-integer levels, is denoted by $\mathcal{M}(k - \tfrac{1}{2}, i)$ and can be written as

$$\mathcal{M}(k - \tfrac{1}{2}, i) = \eta(k - \tfrac{1}{2}, i)\mathcal{M}_B(i), \tag{4}$$

Unauthenticated | Downloaded 12/05/22 01:05 AM UTC

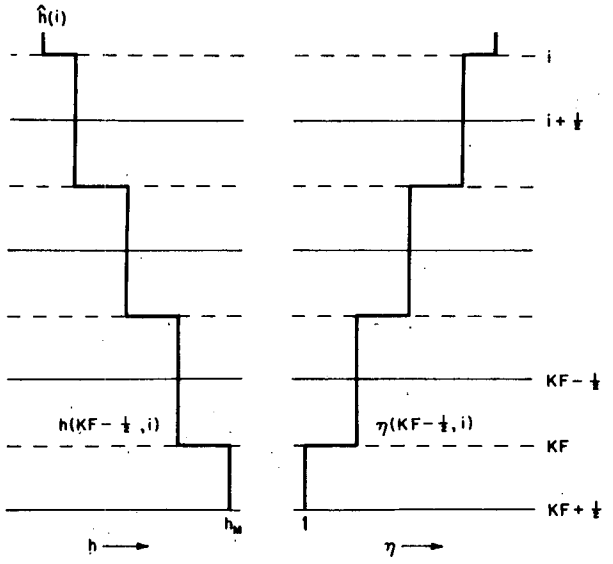


FIG. 3. Typical vertical profiles of normalized vertical mass flux $\eta$ and moist static energy $h$ for the $i$th cloud type. These variables are formally defined at the half-integer levels, e.g., $h(KF - ½, i)$. The cloud-base moist static energy is $h(KF + ½, i) = h_m$ and the subensemble vertical mass flux is $\eta(KF + ½, i) = 1$. The cloud-top moist static energy is denoted by $\hat{h}(i)$.

where $\mathcal{M}_B(i)$ is the cloud-base mass flux for cloud type $i$ and $\eta(k - ½, i)$ is the normalized subensemble vertical mass flux at level $k - ½$. The entrainment of environmental air, denoted by $E(k, i)$, occurs at all integer levels penetrated by the cloud including the cloud top. The detrainment of cloud air, denoted by $D(i)$, occurs only at the cloud-top level. Note that the variables $E(k, i)$ and $D(i)$ represent the total entrainment and detrainment integrated over each layer.

The cumulus cloud ensemble model determines the subensemble thermodynamical properties from the known large-scale thermodynamical structure through the conservation of mass, moist static energy and the total amount of water during entrainment and detrainment processes. In this discrete model, the subensemble thermodynamical properties are represented as step functions in the vertical whose values change due to entrainment at the integer levels. Typical vertical profiles of $\eta(k - ½, i)$ and subensemble moist static energy $h(k - ½, i)$ are shown schematically in Fig. 3. The respective conservation equations can then be integrated from cloud-base to cloud-top level, using a trial value of $\lambda(i)$. The true value of $\lambda(i)$ is obtained iteratively by applying a non-buoyancy condition at the cloud-top level. The subensemble thermodynamical properties at all half-integer levels and the cloud-top level are then determined and the cloud-work function can be calculated. The reader is referred to the discussion of (133) of Part I, (5) of Part II and (3) of Part III for a definition of the cloud-work function and a discussion of its central importance to this cumulus parameterization. The discretized forms of the subensemble budget equations, the iteration procedure for the fractional entrainment rate, and the discretized form of the cloud-work function are presented in the Appendix. A parameterized ice phase, described by Lord (1978), may be included in this model but is not discussed here.

## 3. The mass flux distribution equation

### a. The discretized equation

The mass flux distribution equation for the continuous case is given by (158) of Part I. In discrete numerical prediction models, this equation is integrated over a time step $\Delta t$ and is written as

$$\mathcal{M}_B(i)\Delta t > 0 \quad \text{and}$$

$$\sum_{j=1}^{i_{\max}} [K(i, j)\mathcal{M}_B(j)\Delta t] + F(i)\Delta t = 0, \qquad (5a)$$

or

$$\mathcal{M}_B(i)\Delta t = 0 \quad \text{and}$$

$$\sum_{j=1}^{i_{\max}} [K(i, j)\mathcal{M}_B(j)\Delta t] + F(i)\Delta t < 0, \qquad (5b)$$

for $1 \leqslant i \leqslant i_{\max}$. Here $i_{\max}$ is the number of existing subensembles; $K(i, j)$, for $1 \leqslant i, j \leqslant i_{\max}$, is a discrete form of the mass flux kernel which gives the stabilization of the $i$th subensemble through modification of the large-scale environment by the $j$th subensemble; and $F(i)$ is the large-scale forcing for the $i$th subensemble. The following sections describe algorithms for calculating $F(i)$ and $K(i, j)$ for each $i$ and $j$.

### b. The large-scale forcing

The large-scale forcing for the $i$th subensemble was defined in Part I as the change in cloud-work function due to large-scale processes

$$F(i) = \left[\frac{dA(i)}{dt}\right]_{LS}, \qquad (6)$$

where the subscript $LS$ refers to the large-scale processes. Let us now assume that the cumulus parameterization is applied to a numerical prediction model having a time step $\Delta t$ as noted earlier. Let the large-scale thermodynamical variables (temperature, water vapor mixing ratio, etc.) be denoted collectively by $\bar{\psi}_0$ where the subscript denotes a particular time $t_0$. The effects of the large-scale processes (e.g., large-scale vertical and horizontal advections of temperature and moisture, radiative heating and boundary-layer processes) are applied over $\Delta t$ to give

$$\bar{\psi}' = \bar{\psi}_0 + \left[\frac{\partial \bar{\psi}}{\partial t}\right]_{LS} \Delta t, \qquad (7)$$

Unauthenticated | Downloaded 12/05/22 01:05 AM UTC

where $[\partial\bar{\psi}/\partial t]_{LS}$ represents the time change of $\bar{\psi}$ due to the large-scale processes. Let the cloud-work function for the $i$th subensemble calculated from $\bar{\psi}'$ be denoted by $A'(i)$. Then (6) is written as

$$F(i) = \frac{A'(i) - A_0(i)}{\Delta t} \tag{8}$$

as shown schematically in Fig. 4.

When this cumulus parameterization is used to analyze observational data, as in Part III, $A_0(i)$ may be calculated from data at a given observation time. However, when this parameterization is applied in a prognostic model, $A_0(i)$ can be replaced by a characteristic value for the $i$th subensemble. The replacement of $A_0(i)$ by a characteristic value can be justified as follows. In Part II it was shown that when both large-scale and cloud processes are operating, cloud-work function values calculated from observations in the tropics and subtropics fall into a well-defined narrow range for each subensemble, and the variation in the cloud-work function becomes negligible over the time scale of the large-scale motions. It follows that observed time-mean cloud-work function values may be used as $A_0(i)$ in a large-scale prognostic model. Modification of $\bar{\psi}'$ by the cumulus mass flux obtained from (5) should restore $A'(i)$ to the characteristic value $A_0(i)$. In the UCLA GCM,

$$A_0(i) = A_N(i)[p_B - \hat{p}(i)] \tag{9}$$

is used, where the $A_N(i)$ are calculated from the Marshall Islands data as described by Lord (1978) and are listed in Table 1.

### c. *The mass flux kernel*

The kernel element $K(i, j)$ is defined as the time rate of change of the cloud-work function for the $i$th subensemble due to modification of the large-scale environment by a unit mass flux of the $j$th subensemble. The changes in the large-scale environment

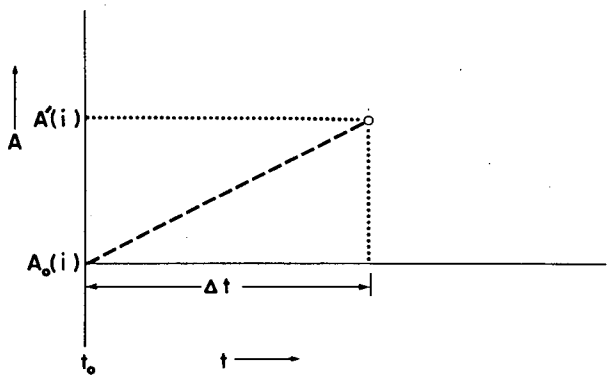


FIG. 4. A schematic diagram showing the change in the subensemble cloud-work function by the large-scale processes over a time $\Delta t$. $A'(i)$ and $A_0(i)$ are defined in the text.

TABLE 1. The average observed cloud-work functions $A_N(i)$ of (9) for each cloud type and the number of observations from the Marshall Islands data set used to determine the averages.

| $\hat{p}(i)$ | $A_N(i)$ | No. of observations |
|---|---|---|
| 150 | 1.6851 | 755 |
| 200 | 1.1686 | 1860 |
| 250 | 0.7663 | 2191 |
| 300 | 0.5255 | 2261 |
| 350 | 0.4100 | 2214 |
| 400 | 0.3677 | 2157 |
| 450 | 0.3151 | 2140 |
| 500 | 0.2216 | 2044 |
| 550 | 0.1521 | 1640 |
| 600 | 0.1082 | 1020 |
| 650 | 0.0750 | 641 |
| 700 | 0.0664 | 407 |
| 750 | 0.0553 | 250 |
| 800 | 0.0445 | 95 |
| 850 | 0.0633 | 7 |

are given by the cumulus terms in the large-scale budget equations (74) and (75) of Part I. These terms are written in discrete form as (A7) in the Appendix. Following the above definition of $K(i, j)$, the large-scale environment, represented by $\bar{\psi}'$ from (7), is modified by an arbitrarily chosen amount of mass per unit area from the $j$th subensemble $\mathcal{M}_B''(j)\Delta t''$ to give

$$\bar{\psi}''(k) = \bar{\psi}'(k) + \delta_j[\bar{\psi}(k)]\mathcal{M}_B''(j)\Delta t''. \tag{10}$$

Here the index $k$ has been added to indicate the level in the large-scale model, $\delta_j[\bar{\psi}(k)]$ refers to the time rate of change in $\bar{\psi}(k)$ per unit mass flux of the $j$th subensemble and is given by (A7) as noted previously, and the double prime denotes a value used in the mass-flux kernel element calculation. A new fractional entrainment rate $\lambda''(i)$ and cloud-work function $A''(i)$ are then calculated for the $i$th subensemble using $\bar{\psi}''$. Finally, the kernel element is calculated as

$$K(i, j) = \frac{A''(i) - A'(i)}{\mathcal{M}_B''(j)\Delta t''}. \tag{11}$$

A procedure similar to (11) is used to calculate the kernel elements in the observational semi-prognostic study described in Part III. However, $A'(i)$ and $\bar{\psi}'$ are replaced by $A_0(i)$ and $\bar{\psi}_0$, which are readily available from observations in the case of a semi-prognostic study. The choice of a particular value for $\mathcal{M}_B''(j)\Delta t''$ is not important provided that it is sufficiently small (but large enough to avoid significant roundoff errors).

Since a given cloud type tends to stabilize the large-scale environment for all cloud types, the kernel elements $K(i, j)$ should be typically negative. In particular, a given subensemble must reduce its own cloud-work function, i.e., for all $i$,

$$K(i, i) < 0. \tag{12}$$

Unauthenticated | Downloaded 12/05/22 01:05 AM UTC

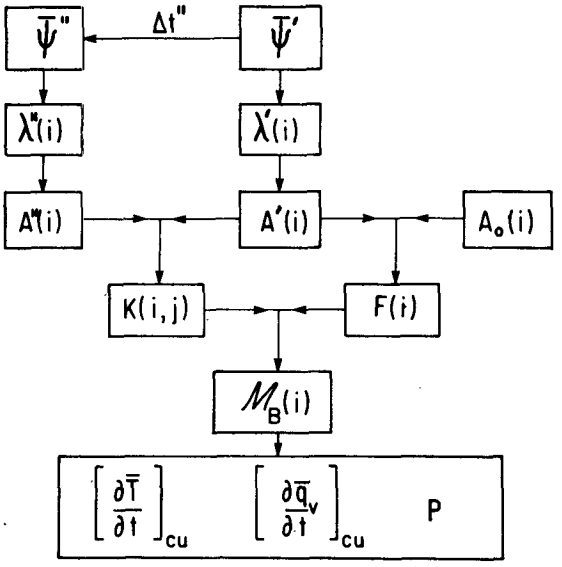


FIG. 5. A schematic diagram showing the procedure used in applying this discretized model of the Arakawa-Schubert parameterization to a prognostic model of the large-scale atmospheric circulations. See text for details.

However, under very unusual circumstances, resulting primarily from too coarse a vertical resolution, the calculated value of $K(i, i)$ may not satisfy this condition. Therefore, $K(i, i) \leqslant -\xi$, where $\xi$ is arbitrarily chosen to be $5 \times 10^{-3}$ J m$^{-2}$ kg$^{-2}$, is enforced. Note that when $i = i_{\max} = 1$, (12) is a necessary condition for $\mathcal{M}_B(i)\Delta t > 0$.

The procedure for obtaining the cloud-base mass flux distribution in a numerical prediction model is summarized in Fig. 5. The thermodynamical variables after modification by the large-scale processes ($\bar{\psi}'$) are inputs to this cumulus parameterization scheme. From these variables $\lambda'(i)$ and $A'(i)$ are calculated for each subensemble. Using an empirically defined cloud-work function $A_0(i)$, the large-scale forcing is calculated from (8). The large-scale environment is then modified by an arbitrary amount of subensemble mass flux $\mathcal{M}'_B(j)\Delta t''$ to produce thermodynamical variables $\bar{\psi}''$ which are then used to calculate a new value of the cloud-work function $A''(i)$. The kernel elements are calculated from (11) and the $\mathcal{M}_B(i)$ are determined from the mass flux distribution equation (5). The next section describes the solution of (5).

## 4. Solution of the mass flux distribution equation

The mass flux distribution equation (5) must be solved subject to the constraints of non-negative $\mathcal{M}_B(i)$ and the inequality conditions (5b) in addition to the usual difficulties associated with the numerical solution of a Fredholm integral equation of the first kind (Courant and Hilbert, 1953, p. 159). Schubert (1973) discussed the difficulties associated with a straightforward solution to this problem; he proposed an initial-value iterative method of solving the equation. Hack and Schubert (1976) and Silva-Dias and Schubert (1977) have discussed the solution of (5) as an optimization problem using linear programming techniques. Here two solution methods are briefly described.

### *a. A direct solution method*

The method proceeds as follows (Fig. 6):

STEP 1: Solve the system of equations (5a) by Gaussian elimination.

STEP 2: Examine the solution, $\mathcal{M}_B(i)\Delta t$ for $1 \leqslant i \leqslant i_{\max}$. If $\mathcal{M}_B(i)\Delta t > 0$ for all $i$, the calculations are terminated.

STEP 3: If $\mathcal{M}_B(i)\Delta t < 0$ for any cloud type these cloud types are ignored in future calculations and step 1 is repeated.

A solution obtained with the above procedure satisfies the equality conditions of (5a) and the conditions of non-negative mass flux. However, the inequality conditions (5b) must also be satisfied for the cloud types with $\mathcal{M}_B(i)\Delta t = 0$. If so, an exact solution of (5) has been determined. In general, however, there is no guarantee that the solution will satisfy the condition (5b). For this reason, and since the direct method includes the rather ambiguous procedure, step 3, it is not desirable for general use. However, when discussing alternative methods of solving the mass flux distribution equation, such as the simplex linear programming method described below, it is useful to compare results to those of the

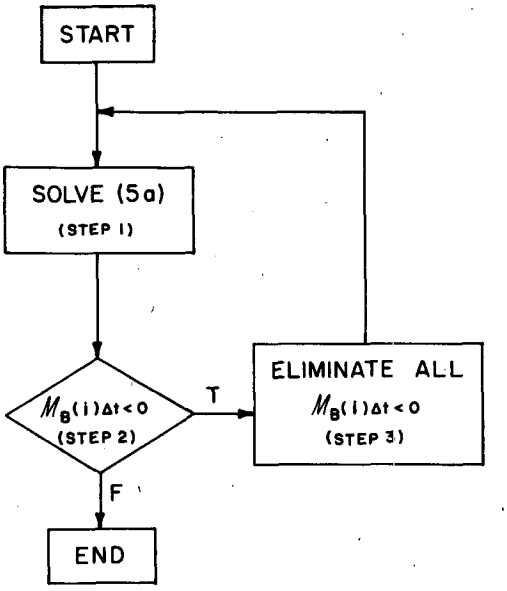


FIG. 6. Flow diagram for the direct solution method for solving the mass flux distribution equation. See text for details.

Unauthenticated | Downloaded 12/05/22 01:05 AM UTC

direct method. Such a comparison is discussed in Part III.

*b. A linear programming method*

The generalized linear programming problem for $l_{max}$ equations and $m_{max}$ unknowns (where $m_{max} \geq l_{max}$) $x(m)$, is stated as follows (Gass, 1975): solve the set of linear equations

$$\sum_{m=1}^{m_{max}} a(l, m)x(m) = b(l) \quad \text{for} \quad 1 \leq l \leq l_{max}, \quad (13)$$

subject to the constraints of

$$x(m) \geq 0 \quad \text{for} \quad 1 \leq m \leq m_{max} \quad (14)$$

and a minimized linear objective function $Z$ defined by

$$Z \equiv \sum_{m=1}^{m_{max}} c(m)x(m). \quad (15)$$

One method of solving this problem is the simplex algorithm (Dantzig, 1963; Gass, 1975). To solve the mass flux distribution equation as a linear programming problem, let $l_{max} = i_{max}$ and $m_{max} = 2i_{max}$. Then let $b(l) = F(l)\Delta t$, $a(l, m) = -K(l, m)$ and $x(m) = \mathcal{M}_B(m)\Delta t$ for $1 \leq l, m \leq l_{max}$. For $l_{max} + 1 \leq m \leq m_{max}$ let $a(l, m)$ be given by

$$a(l, m) = \begin{cases} \pm 1 & \text{for} \quad m = l + l_{max} \\ 0 & \text{for} \quad m \neq l + l_{max} \end{cases} \quad (16)$$

where the choice of + or − is discussed below, and $x(m)$ be $|g(i)|$, where $i \equiv m - l_{max}$ and

$$g(i) \equiv \sum_{j=1}^{i_{max}} [K(i, j)\mathcal{M}_B(j)\Delta t] + F(i)\Delta t. \quad (17)$$

The $g(i)$ are referred to as "slack" variables. As seen from (17) the slack variables represent the deviation of the cumulus stabilization from the large-scale destabilization for each cloud type. They would be identically zero if an exact solution to (5), with all $\mathcal{M}_B(i)\Delta t > 0$, were determined by the simplex algorithm. Let us now rewrite (13) in an expanded form

$$\left.\begin{aligned} &a(1, 1)x(1) + a(1, 2)x(2) + \cdots + a(1, l_{max})x(l_{max}) \pm x(l_{max} + 1) = b(1) \\ &a(2, 1)x(1) + a(2, 2)x(2) + \cdots + a(2, l_{max})x(l_{max}) \pm x(l_{max} + 2) = b(2) \\ &\quad\vdots \\ &a(l_{max}, 1)x(1) + a(l_{max}, 2)x(2) + \cdots + a(l_{max}, l_{max})x(l_{max}) \pm x(m_{max}) = b(l_{max}). \end{aligned}\right\} \quad (18)$$

When the slack variables are preceded by minus signs, the cumulus stabilization, given by the first $l_{max}$ terms on the left-hand side of (18), is always greater than or equal to the destabilization given on the right-hand side. This case is referred to as the "overadjustment" method by Silva-Dias and Schubert (1977). The "underadjustment" method is posed by using plus signs in (18).

The statement of the problem is completed by specifying the coefficients $c(m)$ for $1 \leq m \leq m_{max}$. Obviously,

$$c(m) = 0 \quad \text{for} \quad 1 \leq m \leq l_{max} \quad (19a)$$

is required since the unknown mass fluxes $x(m)$, for $1 \leq m \leq l_{max}$, should not be subject to the minimization constraint on (15). At present the remaining weighting coefficients cannot be determined from any physical principle. Therefore, the slack variables are weighted equally with

$$c(m) = 1.0 \quad \text{for} \quad l_{max} + 1 \leq m \leq m_{max}. \quad (19b)$$

The sensitivity of the simplex solution method to the choice of the $c$'s has been discussed in Part III.

The advantage of the simplex linear programming method is that it produces an optimal solution by minimizing the objective function $Z$. However, it is important to choose the proper signs preceding the slack variables so that the simplex solution is in fact an optimal solution of (5). From (18) and (17) it is evident that the underadjustment method tends to produce $g(i) \geq 0$ for all $i$. However, (5b) requires $g(i) < 0$ whenever $\mathcal{M}_B(i)\Delta t = 0$. Therefore, the underadjustment method should not produce a solution satisfying (5) unless $g(i) = 0$ and $\mathcal{M}_B(i)\Delta t > 0$ for *all* $i$. Experience has shown that these conditions very rarely occur; therefore, the simplex underadjustment solution is not the best solution of the optimization problem. From (18) and (17) it is evident that overadjustment occurs when $g(i) \leq 0$. Therefore, the optimal solution under these conditions will tend to satisfy (5b) whenever $\mathcal{M}_B(i)\Delta t = 0$ and, although (5a) may not be satisfied exactly when $\mathcal{M}_B(i)\Delta t > 0$, the simplex method should produce the optimal solution by minimizing the overadjustment. Results with the simplex and direct solution methods are compared in Part III.

## 5. The cumulus cloud feedback on the large-scale fields

It is a simple procedure to calculate the feedback of the cumulus ensemble on the large-scale environment for given $\mathcal{M}_B(i)\Delta t$. Consider the $k$th layer of

Unauthenticated | Downloaded 12/05/22 01:05 AM UTC

the discrete model. The total temperature and moisture changes at each level over the time $\Delta t$ due to cumulus convection are given by

$$\left[\frac{\partial \bar{T}(k)}{\partial t}\right]_{CU} \Delta t = \sum_{j=1}^{i_{max}} \delta_j[\bar{T}(k)]\mathcal{M}_B(j)\Delta t \quad (20a)$$

and

$$\left[\frac{\partial \bar{q}_v(k)}{\partial t}\right]_{CU} \Delta t = \sum_{j=1}^{i_{max}} \delta_j[\bar{q}_v(k)]\mathcal{M}_B(j)\Delta t, \quad (20b)$$

where the form of $\delta_j$ is given by (A7) in the Appendix. The subsidence at the SCL top is given by

$$-[w_B]_{CU}\Delta t = \sum_{j=1}^{i_{max}} \frac{1}{\rho_B}\mathcal{M}_B(j)\Delta t, \quad (21)$$

where $\rho_B = (p_s - p_B)/(gz_B)$ and $p_s$ is the surface pressure. The amount of precipitation $P\Delta t$ is given by

$$P\Delta t = \sum_{j=1}^{i_{max}} \sum_{k=i}^{KF} c_0 \Delta z(k) q_l(k - \tfrac{1}{2}, i) \times \mathcal{M}(k - \tfrac{1}{2}, i)\Delta t, \quad (22)$$

where $c_0 = 2 \times 10^{-3}$ m$^{-1}$ is an empirically defined conversion (per unit height) of suspended liquid water droplets to precipitation, $\Delta z(k)$ is the thickness of layer $k$, $q_l(k - \frac{1}{2}, i)$ is the suspended liquid water mixing ratio and $\mathcal{M}(k - \frac{1}{2}, i)$ is defined by (4). Lord (1978) has shown that this value of $c_0$ produces good agreement with observed liquid water content in hurricanes summarized by Ackerman (1963). Similar calculations by Schubert (1973) for Marshall Islands data also have shown good agreement with observations. Further details of the precipitation parameterization are found in the Appendix.

## 6. Summary

An application of the Arakawa-Schubert cumulus parameterization to a prognostic model of the large-scale atmospheric circulations has been described. The cloud subensemble properties are determined from the conservation of mass, moist static energy and total water. The large-scale forcing and the mass flux kernel are calculated from changes in the cloud-work function produced by the large-scale processes and the cumulus clouds respectively. Several methods for solving the mass flux distribution equation are described. The predicted distribution of cumulus mass flux is then applied to the large-scale thermodynamical budget equations to determine cumulus feedback on the large-scale environment. The Appendix gives some details which are not described in the main body of the paper.

*Acknowledgments.* We thank Chris Kurasch and Donna Hollingworth for programming assistance, Julia Lueken and Angel Tillman for typing the manuscript and Beverly Gladstone for drafting the figures. Reviewers' comments substantially improved an earlier version of this paper. This research was supported by the National Science Foundation and the National Oceanic and Atmospheric Administration under Grant ATM 78-01922, by the Office of Naval Research through the Naval Environmental Prediction Research Facility under Grant N00014-78-C-0103 and by the National Aeronautics and Space Administration through the Goddard Space Flight Center, Institute for Space Studies, under Grant NGR 05-007-328. Computing assistance was obtained from the UCLA Computing and Information Systems, Campus Computing Services.

## APPENDIX

## The Discrete Cumulus Ensemble Model

This Appendix describes more details of a discrete form of the Arakawa-Schubert cumulus ensemble model. Section 1 gives the discrete form of the subensemble budget equations for mass, moist static energy and total cloud water. Section 2 presents the solution procedure for the subensemble fractional entrainment rate. The discretized form of the cloud-work function is given in Section 3 and the discretized large-scale budget equations are derived in Section 4.

### 1. The subensemble budgets for mass, moist static energy and total water

#### *a. The mass budget*

A discretized form of the subensemble mass budget (95) of Part I for layer $k$, $k \neq i$, can be written as

$$\frac{\eta(k - \tfrac{1}{2}, i) - \eta(k + \tfrac{1}{2}, i)}{\Delta z(k)} = \lambda(i)\eta(k + \tfrac{1}{2}, i),$$

from which

$$\eta(k - \tfrac{1}{2}, i) = \eta(k + \tfrac{1}{2}, i)[1 + \lambda(i)\Delta z(k)]. \quad (A1a)$$

Here $\Delta z(k) = z(k - \frac{1}{2}) - z(k + \frac{1}{2})$. The mass budget for the cloud-top layer $k = i$ is given by

$$d(i) = \eta(i + \tfrac{1}{2}, i)[1 + \lambda(i)\hat{\Delta}z(i)], \quad (A1b)$$

where $d(i)$ is the cloud-top mass detrainment integrated over layer $i$, and normalized by the cloud-base mass flux $\mathcal{M}_B(i)$, and $\hat{\Delta}z(i) = z(i) - z(i + \frac{1}{2})$.

#### *b. The moist static energy budget*

For layer $k$ and cloud type $i$ let $h(k + \frac{1}{2}, i)$ be the subensemble moist static energy before entrainment and let $h(k - \frac{1}{2}, i)$ be the subensemble moist static energy after entrainment (Fig. 3). Then the discretized subensemble moist static energy budget integrated over layer $k$ may be written as

Unauthenticated | Downloaded 12/05/22 01:05 AM UTC

$$\eta(k-\tfrac{1}{2},i)h(k-\tfrac{1}{2},i)=\eta(k+\tfrac{1}{2},i)h(k+\tfrac{1}{2},i)+\lambda(i)\Delta z(k)\eta(k+\tfrac{1}{2},i)\bar{h}(k),$$

from which

$$h(k-\tfrac{1}{2},i)=\frac{h(k+\tfrac{1}{2},i)+\lambda(i)\Delta z(k)\bar{h}(k)}{1+\lambda(i)\Delta z(k)}. \quad \text{(A2a)}$$

When $k=KF$ in (A2a), $h(KF+\tfrac{1}{2},i)\equiv h_m$. In the cloud-top detrainment layer (A2a) becomes

$$\hat{h}(i)=\frac{h(i+\tfrac{1}{2},i)+\lambda(i)\hat{\Delta}z(i)\bar{h}(i)}{1+\lambda(i)\hat{\Delta}z(i)}, \quad \text{(A2b)}$$

where $\hat{h}(i)$ is the moist static energy at the cloud-top. Sequential substitutions of (A2a) into (A2b) with $i+1\leqslant k\leqslant KF$ result in a complicated expression for $\hat{h}(i)$ which depends on the known $h_m$ and $\bar{h}(k)$ for $i\leqslant k\leqslant KF$ and the unknown $\lambda(i)$. By requiring non-buoyancy at the cloud top, i.e. $\hat{h}(i)=\bar{h}^*(i)$, $\lambda(i)$ may be determined iteratively as shown in Section 2 below.

*c. The total water budget*

The budget for total cloud water is calculated in two steps as described below. Let the values of the total cloud water (vapor and suspended liquid water) mixing ratio for layer $k$ and cloud type $i$ be defined as follows: let $q(k+\tfrac{1}{2},i)$ be the value entering layer $k$ from below, $q(k,i)$ the value after entrainment but before the precipitation process, and $q(k-\tfrac{1}{2},i)$ the value after the precipitation process, which also is the value leaving layer $k$. Also, let $q_l(k,i)$ be the cloud suspended liquid water mixing ratio before precipitation, and $q_l(k-\tfrac{1}{2},i)$ the value after the precipitation process has been completed.

The first step in the total cloud water budget calculates $q(k,i)$ from

$$q(k,i)=\frac{q(k+\tfrac{1}{2},i)+\lambda(i)\Delta z(k)\bar{q}(k)}{1+\lambda(i)\Delta z(k)}, \quad \text{(A3)}$$

where $\bar{q}(k)$ is the large-scale total water mixing ratio and is identical to $\bar{q}_v(k)$ when the environment is not supersaturated. When $k=KF$ in (A3), $q(KF+\tfrac{1}{2},i)\equiv q_{vm}$.

The second step in the total water budget calculation determines the amount of precipitation produced in layer $k$ from cloud type $i$. When the cloud is saturated at level $k$ the cloud water vapor mixing ratio $q_v(k,i)$ is calculated from a discretized form of (90) of Part I,

$$q_v(k,i)=\bar{q}_v^*(k)+\frac{\gamma(k)}{[1+\gamma(k)]L}\times[h(k-\tfrac{1}{2},i)-\bar{h}^*(k)],$$

where $\gamma(k)=L/c_p[\partial\bar{q}_v^*(k)/\partial T]_p$. The resulting suspended liquid water mixing ratio before precipitation is $q_l(k,i)=q(k,i)-q_v(k,i)$. Part of $q_l(k,i)$ is converted into precipitation by assuming a constant conversion rate per unit height. Therefore,

$$q_l(k-\tfrac{1}{2},i)=q_l(k,i)-c_0\Delta z(k)q_l(k-\tfrac{1}{2},i),$$

from which

$$q_l(k-\tfrac{1}{2},i)=\frac{q_l(k,i)}{1+c_0\Delta z(k)}. \quad \text{(A4)}$$

At the cloud top, $q_v(i,i)=\bar{q}_v^*(i)$ is required in the absence of virtual temperature effects and (A4) is applied with $k=i$ to determine the cloud-top suspended liquid water mixing ratio $\hat{q}_l(i)\equiv q_l(i-\tfrac{1}{2},i)$. For clouds with tops above 400 mb it is assumed that all detrained suspended liquid water is converted to precipitation. This assumption crudely represents the effect of mesoscale stratiform rain although it cannot account for additional subgrid-scale precipitation due to saturated ascent. All precipitation is assumed to fall directly to the ground in this model.

**2. The solution procedure for $\lambda(i)$**

In the absence of virtual temperature effects the cloud-top non-buoyancy condition for cloud type $i$ is $\hat{h}(i)=\bar{h}^*(i)$, where $\hat{h}(i)$ is given by (A2b). Now let a functional $\mathcal{F}[\lambda(i)]$ be defined by

$$\mathcal{F}[\lambda(i)]=\hat{h}(i)-\bar{h}^*(i),$$

where $\mathcal{F}$ depends on $\lambda(i)$ through $\hat{h}(i)$. Thus the vanishing buoyancy condition is

$$\mathcal{F}[\lambda(i)]=0, \quad \text{(A5)}$$

which is an implicit equation for $\lambda(i)$ and can be solved iteratively by the method of false position (Gerald, 1970). Let $\nu$ be the number of iterations, and let $\lambda_\nu(i)$ be $\lambda(i)$ at the $\nu$th iteration. To begin the iteration $\lambda_1(i)=0$ is used and $\mathcal{F}[\lambda_1(i)]$ is calculated. Then $\mathcal{F}[\lambda_2(i)]$ is calculated with $\lambda_2(i)=i\times 1.0\times 10^{-5}$ m$^{-1}$. This choice of $\lambda_2(i)$ is made empirically to produce fast convergence for shallow clouds with relatively large fractional entrainment rates. For succeeding iterations, $\lambda_{\nu+1}(i)$ for $\nu>1$ is given by

$$\lambda_{\nu+1}(i)=\frac{\lambda_\nu(i)\mathcal{F}[\lambda_{\nu-1}(i)]-\lambda_{\nu-1}(i)\mathcal{F}[\lambda_\nu(i)]}{\mathcal{F}[\lambda_{\nu-1}(i)]-\mathcal{F}[\lambda_\nu(i)]}.$$

The iteration is repeated until $|\mathcal{F}[\lambda_\nu(i)]|\leqslant 5.0$ J kg$^{-1}$ which is equivalent to a cloud-top/environment temperature difference of about $5\times 10^{-3}$ K. The iteration usually converges sufficiently after 5 or 6 iterations.

The solution of (A5) gives $\lambda$ for non-buoyant cloud air at level $i$. However, if the non-buoyancy level is bounded by a positive buoyancy layer above and a shallow negative buoyancy layer below[3] the cloud

[3] For example, immediately above a trade-wind inversion (Nitta, 1975).

Unauthenticated | Downloaded 12/05/22 01:05 AM UTC

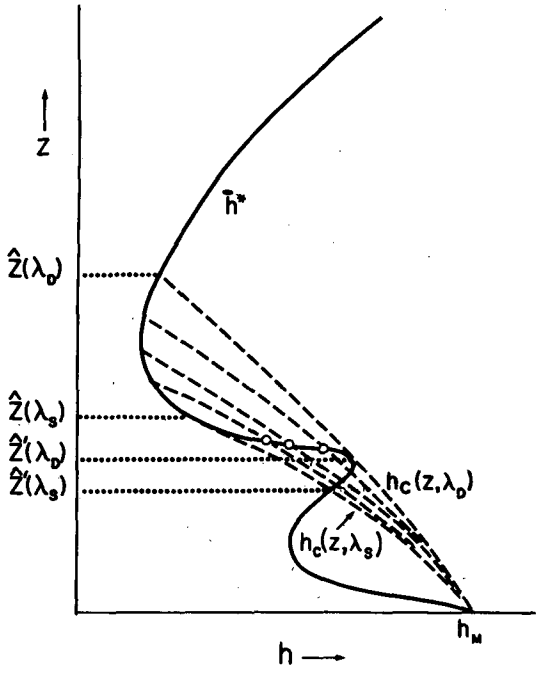


FIG. A1. A schematic diagram of non-buoyancy levels for subensembles with $\lambda$ in the range $\lambda_D < \lambda < \lambda_S$. The open circles represent non-buoyancy levels between $z = \hat{z}(\lambda_S)$ and $z = \hat{z}'(\lambda_D)$ which have a layer of positive buoyancy above. $\hat{z}(\lambda_D)$ and $\hat{z}(\lambda_S)$ are cloud-top non-buoyancy levels for subensembles with $\lambda = \lambda_D$ and $\lambda = \lambda_S$, respectively.

tops will not be at that level. The circled non-buoyancy levels shown in Fig. A1, corresponding to clouds with $\lambda$ in the range $\lambda_D < \lambda < \lambda_S$, are examples of such points in a continuous case. The subscripts $D$ and $S$ denote deep and shallow clouds, respectively. These clouds should have their tops at $\hat{z}(\lambda)$ in the range $\hat{z}(\lambda_S) < \hat{z}(\lambda) < \hat{z}(\lambda_D)$ or $\hat{z}'(\lambda_S) < \hat{z}(\lambda) < \hat{z}'(\lambda_D)$, whereas clouds with $\lambda < \lambda_D$ will have their tops above $\hat{z}(\lambda_D)$ and clouds with $\lambda > \lambda_S$ will have tops below $\hat{z}'(\lambda_S)$.

This situation may occur in the discrete model if the vertical resolution is sufficiently fine to resolve an inversion layer. In Fig. A1, the non-buoyancy levels $\hat{z}(\lambda)$ in the range $\hat{z}'(\lambda_D) < \hat{z}(\lambda) < \hat{z}(\lambda_S)$ for clouds with $\lambda_D < \lambda < \lambda_S$ are a monotonically increasing function of $\lambda$. Therefore, the solution $\lambda(i)$ of (A5) should be rejected as physically unrealistic if the condition $\lambda(i-1) > \lambda(i) > \lambda(i+1)$ holds for a particular value of $i$.

## 3. The cloud-work function

The discretized forms of the large-scale forcing and the mass flux kernel have been defined for the discrete model in Section 3 of the main body of this paper. Both definitions are in terms of the cloud-work function which is defined for the discrete model as

$$A(i) = \sum_{k'=i+1}^{KF+1} \frac{g}{c_p \bar{T}(k'-\tfrac{1}{2})}\,\eta(k'-\tfrac{1}{2}, i) \times\left[\frac{h(k'-\tfrac{1}{2}, i) - \bar{h}^*(k'-\tfrac{1}{2})}{1+\gamma(k'-\tfrac{1}{2})}\right] \times [z(k'-1) - z(k')], \tag{A6}$$

where $z(KF+1) \equiv z_B$.

## 4. The large-scale budget equations

Fig. A2 shows the large-scale budget of $\psi$ ($h$ or $q$) for layer $k$ and cloud type $i$. The downward fluxes of $\bar{\psi}$ per unit cloud-base mass flux at the top and bottom of the layer are given by $\eta(k-\tfrac{1}{2}, i)\bar{\psi}(k-\tfrac{1}{2})$ and $\eta(k+\tfrac{1}{2}, i)\bar{\psi}(k+\tfrac{1}{2})$, respectively. The entrainment of $\bar{\psi}$ is $\lambda(i)\Delta z(k)\eta(k+\tfrac{1}{2}, i)\bar{\psi}(k)$. Let $\delta_i[\bar{\psi}(k)]$ represent a change in $\bar{\psi}(k)$ per unit $\mathcal{M}_B(i)$ and let the mass per unit area of layer $k$ be $\Delta p(k)/g$, where $\Delta p(k) = p(k+\tfrac{1}{2}) - p(k-\tfrac{1}{2})$. Then the large-scale budget of $\psi$ is written as

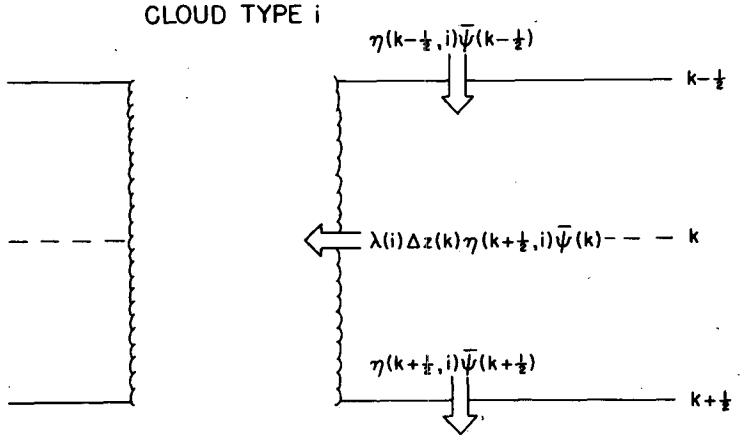


FIG. A2. A schematic diagram of the large-scale budget of $\psi$ for layer $k$ and cloud type $i$.

Unauthenticated | Downloaded 12/05/22 01:05 AM UTC

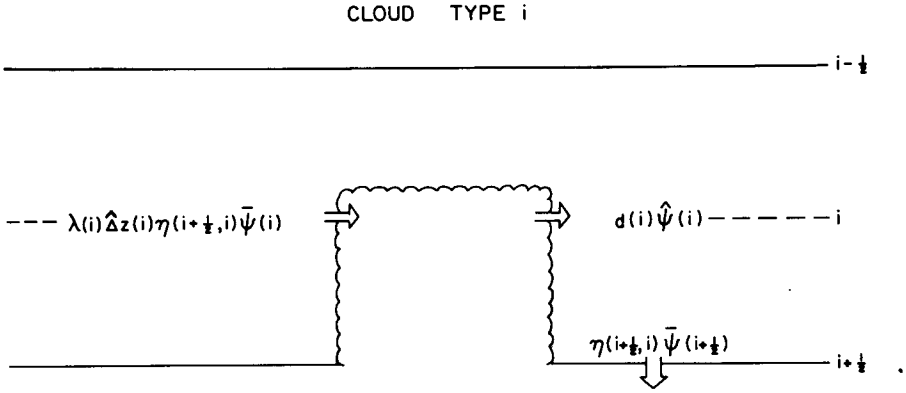


FIG. A3. A schematic diagram of the large-scale budget of $\psi$ for the cloud-top layer for cloud type $i$.

$$\frac{\Delta p(k)}{g}\,\delta_i[\bar{\psi}(k)]$$
$$= \eta(k-\tfrac{1}{2}, i)\bar{\psi}(k-\tfrac{1}{2}) - \eta(k+\tfrac{1}{2}, i)\bar{\psi}(k+\tfrac{1}{2}) - \lambda(i)\Delta z(k)\eta(k+\tfrac{1}{2}, i)\bar{\psi}(k)$$
$$= \eta(k-\tfrac{1}{2}, i)[\bar{\psi}(k-\tfrac{1}{2}) - \bar{\psi}(k)] + \eta(k+\tfrac{1}{2}, i)[\bar{\psi}(k) - \bar{\psi}(k+\tfrac{1}{2})]. \quad \text{(A7)}$$

Fig. A3 shows the large-scale budget of $\psi$ in the cloud-top layer for the $i$th cloud type. At the cloud top the detrainment of $\psi$ per unit $\mathcal{M}_B(i)$ is $d(i)\hat{\psi}(i)$. The downward flux of $\bar{\psi}$ at the bottom of the layer is $\eta(i+\tfrac{1}{2}, i)\bar{\psi}(i+\tfrac{1}{2})$ and the entrainment of $\bar{\psi}$ is $\lambda(i)\hat{\Delta}z(i)\eta(i+\tfrac{1}{2}, i)\bar{\psi}(i)$. Therefore, the counterpart to (A7) for the cloud-top layer is

$$\frac{\Delta p(i)}{g}\,\delta_i[\bar{\psi}(i)] = d(i)\hat{\psi}(i) - \eta(i+\tfrac{1}{2}, i)\bar{\psi}(i+\tfrac{1}{2}) - \lambda(i)\hat{\Delta}z(i)\eta(i+\tfrac{1}{2}, i)\bar{\psi}(i)$$
$$= \eta(i+\tfrac{1}{2}, i)\{[1+\lambda(i)\hat{\Delta}z(i)] \times [\hat{\psi}(i) - \bar{\psi}(i)] + \bar{\psi}(i) - \bar{\psi}(i+\tfrac{1}{2})\}. \quad \text{(A8)}$$

In this model all detrained liquid water is assumed to evaporate instantaneously at the detrainment level. Consequently, the changes in $\bar{T}(k)$ and $\bar{q}_v(k)$ are calculated from $\delta_i[\bar{h}(k)]$ and $\delta_i[\bar{q}(k)]$ as

$$\delta_i[\bar{q}_v(k)] = \delta_i[\bar{q}(k)]$$

and

$$\delta_i[\bar{T}(k)] = \frac{1}{c_p}\{\delta_i[\bar{h}(k)] - L\delta_i[\bar{q}(k)]\}.$$

## REFERENCES


Ackerman, B., 1963: Some observations of water contents in hurricanes. *J. Atmos. Sci.*, **20,** 238–298.

Arakawa, A., and V. R. Lamb, 1977: Computational design of the basic dynamical processes of the UCLA general circulation model. *Methods in Computational Physics*, Vol. 17, Academic Press, 173–265.

——, and W. H. Schubert, 1974: Interaction of a cumulus cloud ensemble with the large-scale environment, Part I. *J. Atmos. Sci.*, **31,** 674–701.

Courant, R., and D. Hilbert, 1953: *Methods of Mathematical Physics*, Vol. 1. Interscience, 560 pp.

Dantzig, G. B., 1963: *Linear Programming and Extensions.* Princeton University Press, 631 pp.

Gass, S., 1975: *Linear Programming: Methods and Applications.* McGraw-Hill, 406 pp.

Gerald, C. F., 1970: *Applied Numerical Analysis.* Addison Wesley, 340 pp.

Hack, J. J., and W. H. Schubert, 1976: Design of an axisymmetric primitive equation tropical cyclone model. Atmos. Sci. Pap. No. 263, Colorado State University, 70 pp.

Lord, S. J., 1978: Development and observational verification of a cumulus cloud parameterization. Ph.D. dissertation, UCLA, 359 pp.

——, 1982: Interaction of a cumulus cloud ensemble with the large-scale environment. Part III: Semi-prognostic test of the Arakawa-Schubert cumulus parameterization. *J. Atmos. Sci.*, **39,** 88–103.

——, and A. Arakawa, 1980: Interaction of a cumulus cloud ensemble with the large-scale environment. Part II. *J. Atmos. Sci.*, **37,** 2677–2692.

Nitta, T., 1975: Observational determination of cloud mass flux distributions. *J. Atmos. Sci.*, **32,** 73–91.

Schubert, W. H., 1973: The interaction of a cumulus cloud ensemble with the large-scale environment. Ph.D. dissertation, UCLA, 168 pp.

Silva-Dias, P. L., and W. H. Schubert, 1977: Experiments with a spectral cumulus parameterization theory. Atmos. Sci. Pap. No. 275, Colorado State University, 132 pp.


Unauthenticated | Downloaded 12/05/22 01:05 AM UTC